

# Implementing Quantum Secret Sharing on Current Hardware

Jay Graves,<sup>1,2,3,\*</sup> Mike Nelson,<sup>2,†</sup> and Eric Chitambar<sup>2,‡</sup>

<sup>1</sup>*Department of Physics, Morehouse College, Atlanta, GA 30314*

<sup>2</sup>*Coordinated Science Laboratory*

*Department of Electrical and Computer Engineering,*

*University of Illinois at Urbana Champaign, Urbana, IL 61801*

<sup>3</sup>*Department of Physics, Yale University, New Haven, CT 06511*

Quantum secret sharing is a cryptographic scheme that enables a secure storage and reconstruction of quantum information. While the theory of secret sharing is mature in its development, relatively few studies have explored the performance of quantum secret sharing on actual devices. In this work, we provide a pedagogical description of encoding and decoding circuits for different secret sharing codes, and we test their performance on IBM's 127-qubit *Brisbane* system. We evaluate the quality of implementation by performing a SWAP test between the decoded state and the ideal one, as well as by estimating how well the code preserves entanglement with a reference system. Results indicate that a  $((3,5))$  threshold secret sharing scheme performs slightly better overall than a  $((5,7))$  scheme based on the SWAP test, but is outperformed by the Steane Code scheme in regards to the entanglement fidelity. We also investigate one implementation of a  $((2,3))$  qutrit scheme and find that it performs the worst of all, which is expected due to the additional number of multi-qubit gate operations needed to encode and decode qutrits.

## I. INTRODUCTION

Securely storing and distributing information is one of the oldest and most important communication tasks. With the advent of quantum computing, traditional cryptographic techniques are being challenged in new and disruptive ways. At the same time, quantum computing also offers a pathway for realizing new cryptographic schemes with potentially stronger security guarantees than their classical counterparts. One such example is quantum secret sharing (QSS) [1], which offers a solution to the problem of distributing secrets among multiple parties.

In classical cryptography, Blakely [2] and Shamir [3] were the first to formally introduce the theory of secret sharing. The most well-known protocols are  $(k, n)$  threshold schemes, in which a secret is divided into  $n$  shares; any  $k$  of those shares can be used to reconstruct the secret, but any fewer number contains no information about the secret. More generally, one constructs codes in which just certain subsets of shares can recover the secret, as specified by the code's access structure. Hillery *et al.* later observed that quantum states could be used for building threshold schemes by encoding a classical secret into a multipartite entangled state [4]. Unlike traditional secret sharing protocols that rely on computational hardness assumptions, the security of ideal quantum-based schemes depends only on the physical principles of quantum mechanics. Going one step further, Cleve *et al.* introduced fully quantum secret sharing protocols [1], which involves the distribution and reconstruction of a quantum secret, i.e. the superposition state of some quantum system. Since these initial works, the theory of

QSS has received heavy development and a wide range of protocols have been proposed [5–20]. Complementing this theory work has been experimental progress on implementing different QSS schemes, primarily in photonic systems [21–29].

These experimental demonstrations involve setups that are designed specifically for the task of secret sharing. However, any functioning quantum computer should be able to run basic QSS protocols. In fact, since every QSS scheme utilizes a type of error correcting code [1], secret sharing is a natural functionality to the demand of a quantum computer on the road toward fault-tolerance. Furthermore, while secret sharing is often described in the scenario of multiple parties separated by some large spatial distance, it also has applications in much smaller computational settings. For example, one can imagine a modular quantum computing architecture in which sensitive data gets distributed onto different zones to minimize a potential data breach. Motivated by these considerations, we investigate the performance of quantum secret sharing codes on current quantum computing hardware. As the simplest possible benchmark, we consider a single-qubit secret, checking whether privacy is attained after encoding and whether the secret is successfully recovered after decoding.

In the following, we begin by reviewing the basic elements of QSS and describing the three codes that we implement; a more comprehensive overview can be found in the work of Gottesman [5]. In Section II, we outline our encoding and decoding methods in more detail and also explain our figure of merits for the code performance. The codes were implemented on IBM's 127-qubit *Brisbane* superconducting processor, and the results are presented in Section IV. In particular, we find that the  $((3,5))$  QSS scheme using the five-qubit code performs the best at passing the SWAP test, while the Steane code is better at preserving entanglement. Results also indi-

\* jay.graves@yale.edu

† minelson@illinois.edu

‡ echitamb@illinois.edu

cate that larger qubit erasures are harder to recover from but improve the ability to preserve entanglement. We also find that the use of matrix-free measurement mitigation (M3) significantly enhances the performance of the QSS protocols and that classical feed-forward is more efficient than fully coherent decoding for QSS schemes. We firmly expect that the performance can be improved even further by employing other error mitigation techniques such as dynamical decoupling [30].

While those familiar with QSS can skip immediately to Section IV for a summary of our results, we adopt a pedagogical approach to the first part of the paper. Our hope is that this not only makes the paper more accessible, but it also allows it to serve as a useful reference for basic QSS circuits.

## II. PRELIMINARIES

Suppose that  $|\psi\rangle = \alpha|0\rangle + \beta|1\rangle$  is an arbitrary qubit state that some “dealer” wishes to distribute to  $n$  parties. If each party itself is given a qubit system, then the dealer performs an encoding isometry  $V : \mathbb{C}^2 \rightarrow \mathbb{C}^n$ , which maps  $|\psi\rangle$  into the  $n$ -qubit state

$$|\psi\rangle \mapsto V|\psi\rangle = |\psi\rangle_L = \alpha|0\rangle_L + \beta|1\rangle_L.$$

Here,  $|i\rangle_L \in \mathbb{C}^n$  (for  $i \in \{0, 1\}$ ) are states forming a basis for a logical qubit in  $\mathbb{C}^n$ . Letting  $2^{[n]}$  denote the power set of  $[n] := \{1, \dots, n\}$ , every QSS scheme is defined by an access structure  $\mathcal{A} \subset 2^{[n]}$  such that:

- (i) Each  $S \in 2^{[n]} \setminus \mathcal{A}$  is called unauthorized and satisfies

$$\rho^S = \text{tr}_{\bar{S}}(|\psi\rangle\langle\psi|_L), \quad (1)$$

where  $\bar{S}$  denotes the set complement of  $S$  and  $\rho^S$  is some fixed state for systems  $S$  that is independent of  $|\psi\rangle$ , i.e. no statistical information about the relative values of  $|\alpha|$  and  $|\beta|$  can be obtained.

- (ii) Each  $S \in \mathcal{A}$  is called authorized, and there exists a decoder  $\mathcal{D}_S$  such that

$$|\psi\rangle\langle\psi| = \mathcal{D}_S(\text{tr}_{\bar{S}}(|\psi\rangle\langle\psi|_L)). \quad (2)$$

A  $((k, n))$  threshold scheme is a special type of QSS in which  $\mathcal{A}$  consists of all subsets having  $k$  or more parties. The first two QSS schemes we investigate are built from  $[[n, m, d]]$  qubit stabilizer codes. Such codes can correct  $t = \lfloor (d-1)/2 \rfloor$  general errors and  $d-1$  erasure errors [31]; hence they represent  $((n-d+1), n)$  threshold QSS schemes. We specifically consider the  $[[5, 1, 3]]$  (“five-qubit”) code [32] and the  $[[7, 1, 3]]$  (“Steane”) CSS code [33, 34], both of which correct two erasure errors and admit  $((3, 5))$  and  $((5, 7))$  threshold schemes, respectively. However, the Steane code can also correct three erasure errors located on certain subsets of qubits, and we also explore this capability. Finally, we test the exemplifying

$((2, 3))$  qutrit QSS scheme presented in Ref. [1], which is a  $[[3, 1, 2]]_3$  CSS code that can correct a single erasure error and detect a single general error (but cannot correct the latter [35]).

### A. General Encoding

The encoding procedure for stabilizer codes can be implemented in different ways. One method is to consider the evolution of the stabilizer. If  $\{g_i\}_{i=1}^{n-m}$  is an independent set of generators for an  $[[n, m, k]]$  stabilizer code and  $\{\bar{Z}_i\}_{i=n-m+1}^n$  are logical  $Z$  operators, then there always exists a Clifford unitary  $U$  that maps  $\{Z_i\}_{i=1}^n$ , stabilizers of the initial  $n$ -qubit state  $|0\rangle^{\otimes n}$ , to  $\{g_i\}_{i=1}^{n-m} \cup \{\bar{Z}_i\}_{i=n-m+1}^n$ , stabilizers of the logical state  $|0\rangle_L$ ; i.e.  $UZ_iU^\dagger = g_i$  for  $i = 1, \dots, n-m$  and  $UZ_iU^\dagger = \bar{Z}_i$ , for  $i = n-m+1, \dots, n$ . One then needs to find an implementation of  $U$  that is compatible with the native gate set for whatever quantum computing hardware device is being used. Our results were obtained on the IBM Brisbane machine, whose standard gate set consists of qubit rotations about the  $\hat{z}$ -axis ( $R_Z(\phi)$ ),  $\pi$  and  $\pi/2$  rotations about the  $\hat{x}$ -axis ( $X$  and  $\sqrt{X}$ ), and the two-qubit echoed cross-resonance gate (ECR) gate. The ECR gate is equivalent to a CNOT up to single-qubit pre-rotations. The qubit rotation matrices about each of the standard axes on the Bloch sphere are given by

$$\begin{aligned} R_X(\theta) &= \begin{bmatrix} \cos(\theta/2) & -i\sin(\theta/2) \\ -i\sin(\theta/2) & \cos(\theta/2) \end{bmatrix} \\ R_Y(\theta) &= \begin{bmatrix} \cos(\theta/2) & -\sin(\theta/2) \\ \sin(\theta/2) & \cos(\theta/2) \end{bmatrix} \\ R_Z(\phi) &= \begin{bmatrix} e^{-i\phi/2} & 0 \\ 0 & e^{i\phi/2} \end{bmatrix}, \end{aligned}$$

and we can realize the  $R_X(\theta)$  and  $R_Y(\theta)$  gates using IBM Brisbane’s native gate set using the following relations

$$\begin{aligned} R_X(\theta) &= R_Z\left(\frac{\pi}{2}\right)\sqrt{X}R_Z(\theta+\pi)\sqrt{X}R_Z\left(\frac{\pi}{2}\right), \\ R_Y(\theta) &= R_Z(\pi)\sqrt{X}R_Z(\theta+\pi)\sqrt{X}. \end{aligned}$$

The design of all circuits was accomplished using Qiskit. Since Qiskit only supports qubit encodings, to implement the  $((2, 3))$  qutrit code, we essentially embedded each qutrit into a two-qubit system, as explained in Section III D.

### B. General Decoding

The general encoding procedure just described takes an initial  $m$ -qubit secret  $|\psi\rangle$  prepared in registers  $n-m+1, \dots, n$  and maps it into an  $n$ -qubit logical state. In QSS, the secret is recovered after discarding an unauthorized subset of parties. To explain how this is accomplished in practice, let us first describe in more detail

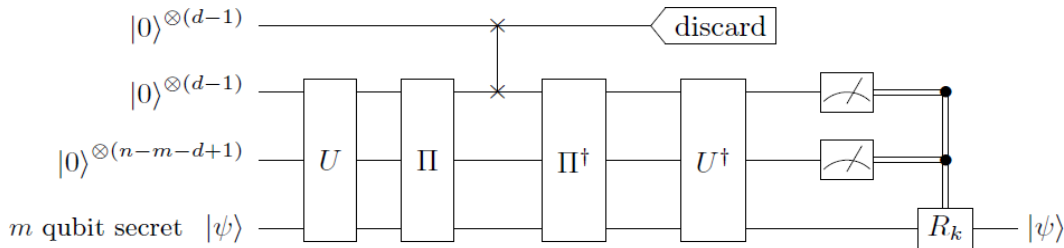


FIG. 1: A general threshold QSS circuit implementation using an  $[[n, m, d]]$  stabilizer code. An arbitrary  $m$ -qubit secret  $|\psi\rangle$  is encoded into  $n$  qubits by a unitary  $U$ . A permutation  $\Pi$  is performed to select an unauthorized set of  $d - 1$  qubits that get discarded. A fresh set of qubits is swapped in place of the latter qubit, and the encoding map is reversed. Finally, an error syndrome is obtained by measuring the  $n - m$  qubits in the computational basis and the appropriate correction  $R_k$  is performed on the unmeasured qubits to recover the secret  $|\psi\rangle$ . Note that the error correction  $R_k$  will depend on the permutation  $\Pi$ .

the error correction procedure for an erasure event. Suppose it is known that some specific physical qubits are lost in a computation or protocol. Some physical reasons for loss are described in Ref. [36], but in QSS the loss is an artifact of the task itself: an authorized subset of parties participate collaboratively to recover the secret, and the remaining qubits are effectively lost since they are held by non-participating parties. To recover the secret, the authorized parties replace the lost qubits with fresh qubits, each in some initial state  $|0\rangle$ . When qubit  $Q_i$  is lost and replaced by qubit  $A_i$ , its mathematical description is described by the completely positive trace-preserving (CPTP) map

$$\begin{aligned} \mathcal{D}^{Q_i \rightarrow A_i}(X^{Q_i}) &= \text{tr}[X^{Q_i}]|0\rangle\langle 0|^{A_i} \\ &= |0\rangle\langle 0|X^{Q_i}|0\rangle\langle 0|^{A_i} + |0\rangle\langle 1|X^{Q_i}|1\rangle\langle 0|^{A_i}, \end{aligned}$$

where we have provided one representation of the map in terms of Kraus operators  $K_0 = {}^{A_i}|0\rangle\langle 0|^{Q_i}$  and  $K_1 = {}^{A_i}|0\rangle\langle 1|^{Q_i}$ . If a code can correct arbitrary errors on qubit  $Q_i$ , then it can also correct the erasure map  $\mathcal{E}^{Q_i \rightarrow A_i}$  by transferring the error correction procedure from system  $Q_i$  to  $A_i$ . The overall effect is that qubits  $Q_i$  and  $A_i$  get swapped in between the encoding and decoding procedure (see Fig. 1).

The standard method for decoding stabilizer codes is to first measure a complete set of generators for the stabilizer, the outcomes of which uniquely identify an error syndrome. The error is then reversed and the inverse of the encoding gate,  $U^\dagger$ , is applied to recover the secret  $|\psi\rangle$ . More explicitly, if  $\{g_i\}_i$  are generators for the stabilizer and  $\{E_k\}_k$  are correctable Pauli errors, then each  $E_k$  has the error syndrome determined by the bit string  $\mathbf{b}_k = (b_{k,i})_i$  such that  $E_k g_i E_k^\dagger = (-1)^{b_{k,i}} g_i$ . The error syndrome is obtained by measuring each of the generators  $g_i$ , and if the syndrome is  $\mathbf{b}_k$ , then the error can be corrected by performing  $E_k^\dagger$  or any other  $E_l^\dagger$  having the same syndrome. Afterward,  $U^\dagger$  is applied to recover the secret  $|\psi\rangle$  in registers  $n - m + 1, \dots, n$ . Equivalently,

since

$$\begin{aligned} (-1)^{b_{k,i}} U^\dagger g_i U &= U^\dagger E_k U (U^\dagger g_i U) U^\dagger E_k^\dagger U \\ \Leftrightarrow (-1)^{b_{k,i}} Z_i &= (U^\dagger E_k U) Z_i (U^\dagger E_k^\dagger U), \end{aligned} \quad (3)$$

one can first evolve the circuit by  $U^\dagger$  prior to the syndrome measurement. The syndrome  $\mathbf{b}_k$  can then be determined by measuring each of the qubits  $l = 1, \dots, n - m$  in the computational basis, and the corresponding error correction is facilitated by performing  $U^\dagger E_k^\dagger U$ . For a distance  $d$  stabilizer code and arbitrary subset  $T$  of  $d - 1$  parties, it suffices to consider just the set of Pauli errors  $\{E_k\}_k = \{\mathbb{I}, X, Y, Z\}^{\times(d-1)}$  acting on qubits in  $T$ . Notice that since  $U$  is a Clifford gate, each  $U^\dagger E_k^\dagger U$  will also be a local Pauli operator. We let  $R_k$  denote the part of  $U^\dagger E_k^\dagger U$  acting on the  $m$ -qubit system recovering the secret, and for simplicity we ignore resetting the other  $n - m$  systems to their original state  $|0\rangle^{\otimes(n-m)}$ . The overall encoding and decoding scheme is depicted in Fig. 1.

### C. Initializing a secret

A  $d$ -dimensional quantum secret is an arbitrary state in  $\mathbb{C}^d$ . For qubits we can parametrize the secret as  $|\psi\rangle = \alpha|0\rangle + \beta|1\rangle = \cos(\theta/2)|0\rangle + \sin(\theta/2)e^{i\phi}|1\rangle$ . The use of rotation gates, specifically  $R_X(\theta)$  and  $R_Z(\phi)$  rotate the state around the Bloch sphere depending on the angles  $\theta$  and  $\phi$ . This allows us to initialize a random secret when we randomize the input angles of the rotation gates, as depicted in Fig. 2a.

More specifically, we arranged  $\theta$  and  $\phi$  into arrays with intervals  $[0, \pi]$  and  $[0, 2\pi]$  respectively, both with a step of  $1^\circ$ . With each circuit job, a random angle is selected from each array and used for the angles of the rotation gates, thus initializing an arbitrary quantum state or secret.

For the qutrit scheme, we embed a three-level system into the space of two qubits;  $|\psi\rangle \in \mathbb{C}^3 \leftrightarrow |\phi\rangle \in \mathbb{C}^2 \otimes \mathbb{C}^2$ , while ignoring one of the basis states of  $\mathbb{C}^2 \otimes \mathbb{C}^2$ .

Specifically, we map a qutrit into two qubits using the mapping

$$|0\rangle \leftrightarrow |00\rangle, \quad |1\rangle \leftrightarrow |01\rangle, \quad |2\rangle \leftrightarrow |10\rangle. \quad (4)$$

Under the qutrit embedding of Eq. (4), we can initialize an arbitrary qutrit state  $|\psi\rangle$  using  $R_Y(\theta)$  and CNOT gates as depicted below. It is straightforward to verify that  $|\psi\rangle = \alpha|0\rangle + \beta|1\rangle + \gamma|2\rangle := \alpha|00\rangle + \beta|01\rangle + \gamma|10\rangle$  where  $\alpha = \cos(\theta_2/2)$ ,  $\beta = \sin(\theta_2/2)\cos(\theta_1)$ , and  $\gamma = \sin(\theta_2/2)\sin(\theta_1)$ .

#### D. Measures of performance

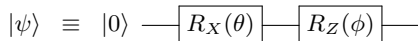
We consider two different ways of evaluating how well a quantum circuit implements a QSS scheme. The first uses the SWAP test, which is a computational primitive shown in Fig. 3. The probability of measuring  $|0\rangle$  is given by  $1/2(1 + |\langle\psi|\phi\rangle|^2)$ , which becomes unity iff the states are the same. Hence, our test will involve (i) randomly selecting angles  $\theta$  and  $\phi$  for the initial qubit state  $|\psi\rangle$ , (ii) preparing two copies of  $|\psi\rangle$ , (iii) running the QSS encoding and decoding on one of the copies, and (iv) performing the SWAP test with the original unencoded state.

The second quantifier of performance for a QSS involves the entanglement fidelity, which for a general quantum channel  $\mathcal{N}$  is defined as

$$F_e(\mathcal{N}) := \langle\Phi^+|(\text{id} \otimes \mathcal{N})(|\Phi^+\rangle\langle\Phi^+|)|\Phi^+\rangle, \quad (5)$$

where  $|\Phi^+\rangle = \sqrt{1/2}(|00\rangle + |11\rangle)$ . Intuitively, the entanglement fidelity measures how well the channel  $\mathcal{N}$  preserves the maximally entangled state  $|\Phi^+\rangle$  when acting on one of the subsystems. In our case, we consider  $\mathcal{N}$  as the concatenation of the QSS encoding  $V$  and the decoding  $\mathcal{D}_S$  after erasing shares in subset  $S$ . Ideally,  $|\Phi^+\rangle$  should be perfectly preserved after encoding and

(a)



(b)

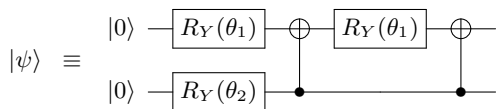


FIG. 2: (a) Initialization of arbitrary qubit quantum state. (b) Initialization of arbitrary qutrit quantum state using qubits.

decoding. For  $d$ -dimensional codes, we replace  $|\Phi^+\rangle$  with  $|\Phi_d^+\rangle = \frac{1}{\sqrt{d}}\sum_{i=1}^d |ii\rangle$  in Eq. (5).

To estimate the entanglement fidelity for a given subset erasure, we perform quantum state tomography on the output state when starting with  $|\Phi^+\rangle$ . Quantum state tomography (QST) is a method for experimentally reconstructing the quantum state from measurement data. QST requires multiple measurements of the quantum system in different bases. For a system of  $n$  qubits, there are  $3^n$  possible measurement bases (corresponding to measurements along the  $X$ ,  $Y$ , and  $Z$  axes for each qubit). Qiskit offers a native QST command, called StateTomography, which we employed in collecting our data.

#### E. Error mitigation

The digital units of a quantum computer (qubits, typically) are very fragile and subject to noise and errors in computation. In the long-term vision of quantum computers, fully fault-tolerant devices can suppress noise and errors to an arbitrarily small degree. However, such low error-rate devices require substantial physical resources. In the present regime of so-called Noisy Intermediate Scale Quantum (NISQ) computation, various strategies for error mitigation have been suggested and demonstrated. These approaches provide some benefits beneath fault-tolerance, without scaling up physical device requirements.

One such approach is matrix-free measurement mitigation (Mthree or M3), which specifically focuses on measurement errors [37]. M3 relies on probabilistic methods to estimate and correct errors. These methods can introduce approximations that may not fully capture the complexity of the noise profile, leading to less accurate corrections compared to full matrix methods. Moreover, the calibration phase in M3 typically involves measuring only a subset of possible error configurations (e.g., single-qubit or pairwise errors). This can miss higher-order correlations between errors on multiple qubits, reducing the effectiveness of the mitigation. Otherwise, M3 is an efficient routine and is a promising technique for obtaining accurate experimental results for large quantum systems, where the number of possible measurement outcomes grows exponentially. A more detailed description of M3 can be found in Ref. [37].

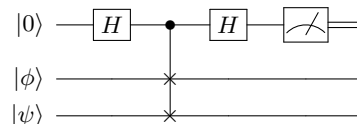


FIG. 3: Quantum SWAP test circuit diagram.

TABLE I: Stabilizer generators for the 5-qubit code.

Element	Operator
$G_1$	$XZZXI$
$G_2$	$IXZZX$
$G_3$	$XIXZZ$
$G_4$	$ZXIXZ$
$\bar{X}$	$XXXXX$
$\bar{Z}$	$ZZZZZ$

### III. SPECIFIC EXAMPLES

#### A. ((3,5)) QSS using the five-qubit code

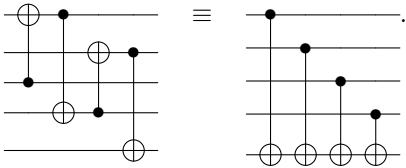
We now apply the general method outlined in Section II to the  $[[5, 1, 3]]$  five-qubit code. Generators for the stabilizer of this code are given in Table I. Our first task is to identify the encoding unitary  $U$  that maps the initial stabilizers  $\{Z_i\}_{i=1}^5$  to the  $\{G_i\}_{i=1}^4 \cup \{\bar{Z}\}$  in Table I. This mapping can be constructed by observing that the generators of the five-qubit code closely resemble the stabilizers for the five-qubit ring state [9]. The latter is represented by a ring graph, and it is generated by performing a controlled- $Z$  (CZ) between adjacent nodes on the graph, each initially in the state  $|+\rangle$  (and hence stabilized by  $X$ ). Applying the same CZ gates on the five-qubit code transforms its generators as

$$\begin{pmatrix} G_1 \\ G_2 \\ G_3 \\ G_4 \\ \bar{Z} \end{pmatrix} \mapsto \begin{pmatrix} XIIXI \\ IXIIX \\ XIXII \\ IXIXI \\ IIIIZ \end{pmatrix}. \quad (6)$$

Noting that CNOT converts  $X_c X_t \mapsto X_c$  and  $Z_c Z_t \mapsto Z_t$  for control ( $c$ ) qubit and target ( $t$ ) qubit. Hence, by applying CNOT to the appropriate pairs of qubits, the generators further transform as

$$\begin{pmatrix} XIIXI \\ IXIIX \\ XIXII \\ IXIXI \\ ZZZZZ \end{pmatrix} \mapsto \begin{pmatrix} XIIII \\ IXIII \\ IIXII \\ IIIXI \\ IIIIZ \end{pmatrix}. \quad (7)$$

Two equivalent circuits realizing this transformation are the following



Then by applying Hadamard gates to qubits 1, 2, 3, and 4, we get

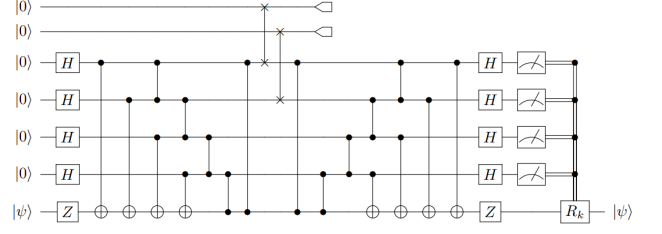


FIG. 4: A circuit implementation of a five-qubit QSS protocol.

$$\begin{pmatrix} XIIII \\ IXIII \\ IIXII \\ IIIXI \\ IIIIZ \end{pmatrix} \mapsto \begin{pmatrix} ZIIII \\ IZIII \\ IIZII \\ IIIZI \\ IIIIZ \end{pmatrix}.$$

Applying these transformations in reverse defines the encoding unitary  $U$ , as depicted in Fig. 4. Here, we have chosen the permutation  $\Pi$  among the unauthorized set to be trivial for convenience.

The next step is to identify the Pauli correction  $R_k$  for each error syndrome  $\mathbf{b}_k$ . This is done by observing how the Pauli errors on the first and second qubits evolve during the application of  $U^\dagger$ . The necessary correction  $R_k$  on the fifth qubit is summarized in Table II. Finally, we perform the fidelity tests to see how well the procedure works at recovering an arbitrary initial secret  $|\psi\rangle$ . Our results are presented in Section IV.

#### B. ((5,7)) QSS using the Steane code

We now apply the same general method to the  $[[7, 1, 3]]$  Steane code. Generators for the stabilizer of this code are given in Table III. As stated previously, CNOT converts  $X_c X_t \mapsto X_c$  and CZ converts  $Z_c Z_t \mapsto Z_t$ . Therefore by applying CNOT to the appropriate pairs of qubits, the generators transform as follows

$$\begin{pmatrix} G_1 \\ G_2 \\ G_3 \\ G_4 \\ G_5 \\ G_6 \\ \bar{Z} \end{pmatrix} \mapsto \begin{pmatrix} IIIIXXX \\ IIIIXXX \\ IIIIXIX \\ IIIZIII \\ IZZIIII \\ IIZIIII \\ IZZZIII \end{pmatrix}.$$

Applying Hadamard gates to qubits 5, 6, and 7, and then multiplying qubit 1 by  $Z$  yields the transformation

	$\mathbb{I}_2$	$X_2$	$Y_2$	$Z_2$
$\mathbb{I}_1$	syndrome = (0,0,0,0) correction $\mathbb{I}_5$	syndrome = (1,0,1,0) correction $X_5$	syndrome = (1,1,1,0) correction $X_5$	syndrome = (0,1,0,0) correction $\mathbb{I}_5$
$X_1$	syndrome = (1,0,1,1) correction $Y_5$	syndrome = (0,0,0,1) correction $Z_5$	syndrome = (0,1,0,1) correction $Z_5$	syndrome = (1,1,1,1) correction $Y_5$
$Y_1$	syndrome = (0,0,1,1) correction $Y_5$	syndrome = (1,0,0,1) correction $Z_5$	syndrome = (1,1,0,1) correction $Z_5$	syndrome = (0,1,1,1) correction $Y_5$
$Z_1$	syndrome = (1,0,0,0) correction $\mathbb{I}_5$	syndrome = (0,0,1,0) correction $X_5$	syndrome = (0,1,1,0) correction $X_5$	syndrome = (1,1,0,0) correction $\mathbb{I}_5$

TABLE II: For arbitrary Pauli errors on qubits one and two in the ((3,5)) QSS scheme, this table provides the unitary correction  $R_k$  on qubit five for each syndrome measurement  $\mathbf{b}_k$ .

$$\begin{pmatrix} IIIIXXX \\ IIIIXXX \\ IIIIXIX \\ IIIZIII \\ IZZIIII \\ IIZIIII \\ IZZZIII \end{pmatrix} \mapsto \begin{pmatrix} ZIIIZZZ \\ ZIIIZZZ \\ ZIIIZIZ \\ ZIIZIII \\ ZZZIIII \\ ZIZIIII \\ ZZZZIII \end{pmatrix}.$$

By adding together different combinations of the generators, it is straightforward to verify that this stabilizes the state  $|0\rangle^{\otimes 7}$ , as desired.

As was the case with the ((3,5)) scheme, applying these transformations in reverse defines the encoding unitary,  $U$ , that maps the initial stabilizers  $\{Z_i\}_{i=1}^7$  to the  $\{G_i\}_{i=1}^6 \cup \{\bar{Z}\}$  as depicted in Fig. 5a. We have chosen the unauthorized set to be the sixth and seventh qubits. The necessary correction  $R_k$  on the first qubit is summarized in Table IV.

### C. More authorized sets using the Steane code

The Steane code enables a more intricate QSS access structure than just a ((5,7)) threshold scheme [38]. As shown in Appendix A, the code can still recover when certain subsets of three qubits are erased (but not all). The encoding is the same, but a slightly different recovery is needed. Figure 5b depicts one such circuit in which qubits one through four form an authorized set. The necessary correction  $R_k$  on the first qubit for all possible syndromes is presented in Appendix A.

TABLE III: Stabilizer generators for the 7-qubit code.

Element	Operator
$G_1$	IIIIXXXX
$G_2$	IXXIIXX
$G_3$	XIXIXIX
$G_4$	IIIZZZZ
$G_5$	IZZIIZZ
$G_6$	ZIZIZIZ
$\bar{X}$	XXXXXXX
$\bar{Z}$	ZZZZZZZ

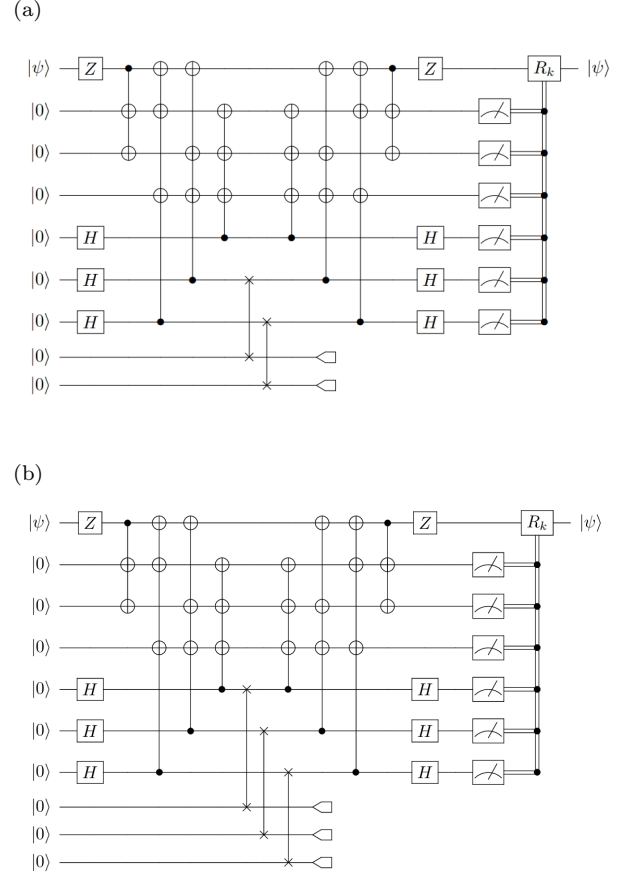


FIG. 5: (a) A circuit implementation of a Seven-qubit (Steane) QSS protocol with two qubits being erased. (b) A circuit implementation of a Seven-qubit (Steane) QSS protocol with three qubits being erased.

### D. ((2,3)) QSS qutrit code

The qutrit scheme involves secrets of the form  $|\psi\rangle = \alpha|0\rangle + \beta|1\rangle + \gamma|2\rangle$ . The secret sharing process was laid out in Cleve *et al.* [1]. While qutrit protocols are not ideally suited for qubit-based hardware, it is still possible to implement them. In this work, we have adopted the

	$\mathbb{I}_7$	$X_7$	$Y_7$	$Z_7$
$\mathbb{I}_6$	syndrome = (0,0,0,0,0,0) correction $\mathbb{I}_1$	syndrome = (0,1,1,0,0,0) correction $X_1$	syndrome = (0,1,1,0,0,1) correction $X_1$	syndrome = (0,0,0,0,0,1) correction $\mathbb{I}_1$
$X_6$	syndrome = (1,0,1,0,0,0) correction $X_1$	syndrome = (1,1,0,0,0,0) correction $\mathbb{I}_1$	syndrome = (1,1,0,0,0,1) correction $\mathbb{I}_1$	syndrome = (1,0,1,0,0,1) correction $X_1$
$Y_6$	syndrome = (1,0,1,0,1,0) correction $X_1$	syndrome = (1,1,0,0,1,0) correction $\mathbb{I}_1$	syndrome = (1,1,0,0,1,1) correction $\mathbb{I}_1$	syndrome = (1,0,1,0,1,1) correction $X_1$
$Z_6$	syndrome = (0,0,0,0,1,0) correction $\mathbb{I}_1$	syndrome = (0,1,1,0,1,0) correction $X_1$	syndrome = (0,1,1,0,1,1) correction $X_1$	syndrome = (0,0,0,0,1,1) correction $\mathbb{I}_1$

TABLE IV: For arbitrary Pauli errors on qubits six and seven in the ((5,7)) QSS scheme, this table provides the unitary correction  $R_k$  on qubit one for each syndrome measurement  $\mathbf{b}_k$ .

following logical encoding

$$\begin{aligned}
|\tilde{\psi}\rangle_L &= \alpha|\tilde{0}\rangle_L + \beta|\tilde{1}\rangle_L + \gamma|\tilde{2}\rangle_L \\
&= \frac{\alpha}{\sqrt{3}}(|000\rangle + |111\rangle + |222\rangle) \\
&+ \frac{\beta}{\sqrt{3}}(|012\rangle + |120\rangle + |201\rangle) \\
&+ \frac{\gamma}{\sqrt{3}}(|021\rangle + |102\rangle + |210\rangle)
\end{aligned} \tag{8}$$

The secret can be reconstructed from any two of the three shares. Given the first two shares (for instance), the recovery unitary  $R_{12}$  involves adding the value of the first share to the second (modulo three), and then adding the value of the second share to the first. This yields the state [1]

$$\begin{aligned}
(R_{12} \otimes I_3)|\tilde{\psi}\rangle_L &= \frac{\alpha}{\sqrt{3}}(|000\rangle + |021\rangle + |012\rangle) \\
&+ \frac{\beta}{\sqrt{3}}(|112\rangle + |100\rangle + |121\rangle) \\
&+ \frac{\gamma}{\sqrt{3}}(|221\rangle + |212\rangle + |200\rangle) \\
&= |\psi\rangle \otimes \frac{1}{\sqrt{3}}(|00\rangle + |12\rangle + |21\rangle),
\end{aligned}$$

which recovers the secret in the first qutrit share. The reconstruction procedure for the other cases is similar ( $R_{23}$  and  $R_{31}$ ), by the symmetry of mapping Eq. (8) with respect to cyclic permutations of the three qutrits [1]. Realizing the recovery unitary transformation,  $R_{ij}$ , for our circuit amounts to numerous SWAP gates (equivalently three CNOT gates), which results in a much more complex circuit compared to the previous QSS schemes. Furthermore, it should be noted that the construction of the qutrit scheme does not follow the same stabilizer approach as the ((3,5)) and ((5,7)) scheme, and does not utilize mid-circuit measurements or classical feed-forwarding. The circuit for our qubit version of the qutrit scheme is shown in Fig. 6.

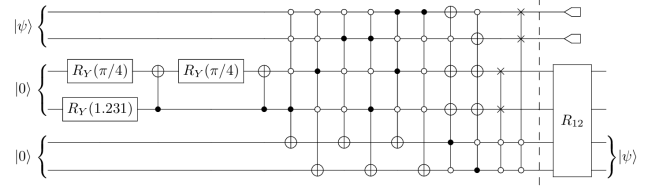


FIG. 6: A circuit implementation of a 3-qutrit QSS protocol (using qubits). The first qutrit is represented by the lower pair of qubits, the second by the middle pair, and so on.

## IV. RESULTS

We now present experimental results for the performance of the above scheme using IBM’s 127-qubit Brisbane system as the experimental platform. We compare our real hardware results with theoretical expectations from simulating noisy circuits using Qiskit’s fake backend *FakeBrisbane*, which runs on a classical computer. Fake backends are constructed to mimic the behaviors of real IBM quantum devices using system snapshots. The system snapshots contain important information about the quantum system such as basis gates, coupling map, gate error rates, and decoherence times (e.g.  $T_1$  and  $T_2$ ). Measurements from the actual quantum system with no error mitigation are denoted as “Real,” while the mitigated real data is denoted as “Real (M3).” Furthermore, the (noisy) simulated and mitigated simulated data are “Sim” and “Sim (M3)” respectively. M3 works with quasi-probability distributions, however, in our case, a true probability distribution is a bit more useful. Therefore we take the returned quasi-probability distribution and map it to the closest probability distribution as defined by the  $L_2$ -norm.

Ten jobs were run for each scheme, each using 1024 shots, thus totaling  $\sim 10000$  shots for each scheme. Each job also used arbitrary initialization angles for the quantum states. We first evaluated the secret recovery by performing a SWAP test as described in Section IID. The figure of merit is the sample rate over 1024 shots of measuring the  $|0\rangle$  state in the SWAP test, which occurs with probability one when the initial and final states are identical. We then estimated the entanglement fi-

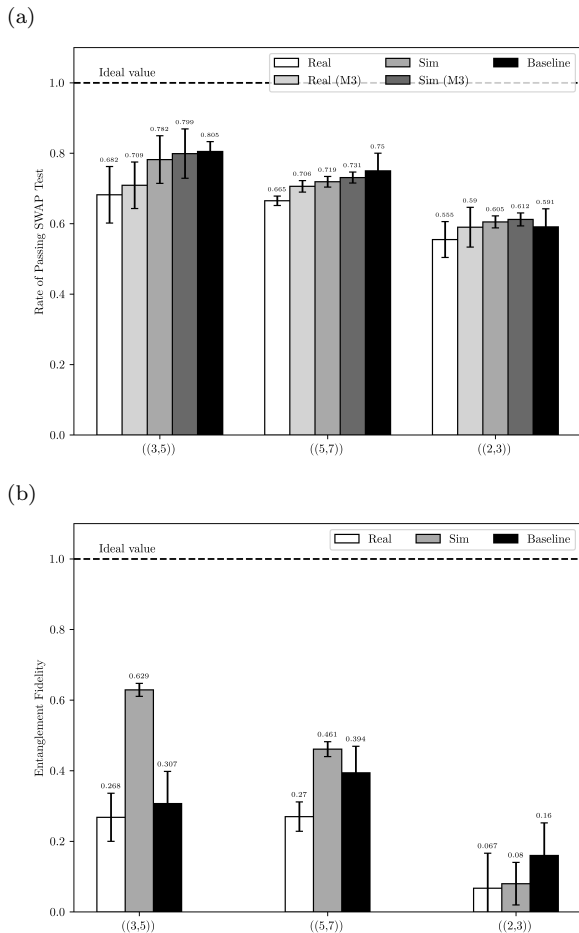


FIG. 7: (a) Sample rate of passing the SWAP test for QSS schemes on the IBM Quantum Brisbane system and corresponding noisy simulators, with and without M3 error mitigation. (b) Entanglement fidelity for QSS schemes using the IBM Quantum Brisbane system and corresponding noisy simulators. For both figures of merit, the ideal value is the noiseless case, meaning the value measured if the schemes are run without noise present. The error bars shown correspond to a 99% confidence interval.

delity of the encoding and decoding process for a given subset of erasures using state tomography. We also determined a “baseline” estimate of our two measures of performance tailored for each circuit’s depth. To do this we placed a sequence of identity gates to obtain a depth similar to that of the corresponding scheme. In other words, we prepared  $|\psi\rangle|\psi\rangle$ , did nothing (placed identities), and then ran the SWAP test; likewise, we prepared  $|\Phi^+\rangle$ , did nothing and then estimated the entanglement fidelity. While this method should work as expected on an ideal quantum computer, in practice the idle qubit(s) will undergo significant decoherence prior to the SWAP test or tomographic reconstruction. We believe this is the primary source of error in the collected data described below. Suggested steps for improvement in future work are described in Section V.

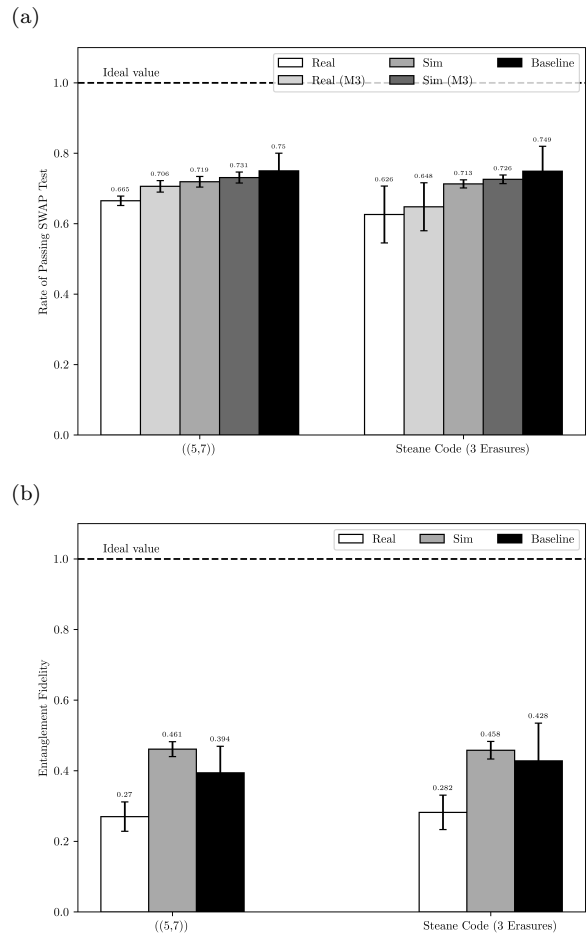


FIG. 8: (a) Sample rate of passing the SWAP test for the Steane code with two and three erasure errors with and without M3 error mitigation. Qubits {6,7} were erased in the two-erasure case, and qubits {5,6,7} were erased in the three-erasure case. (b) Entanglement fidelity for the Steane code with two and three erasure errors. For both figures of merit, the ideal value is the noiseless case, meaning the value measured if the schemes are run without noise present. The error bars shown correspond to a 99% confidence interval.

For the ((3,5)) scheme we evaluated two variations of the circuit: a mid-circuit measurement (MCM) and a delayed circuit measurement (DCM). MCMs utilize measurements that execute before the end of the circuit, while DCMs only utilize measurements at the end of the circuit. Finally, for the Steane code QSS scheme, we evaluated the performance of the code with two and three-qubit erasures. For the three-qubit erasures, we looked at erasing sets of unauthorized and authorized sets, i.e. erasures that do and do not allow recovery.

We can see from Fig. 7a that the ((3,5)) scheme was the most successful at decoding the secret for the SWAP test, followed by the ((5,7)) and ((2,3)) schemes. The ((2,3)) scheme’s performance is somewhat expected due to the complexity of the transpiled circuit, as it contains many multi-qubit gates. Nevertheless, all schemes per-



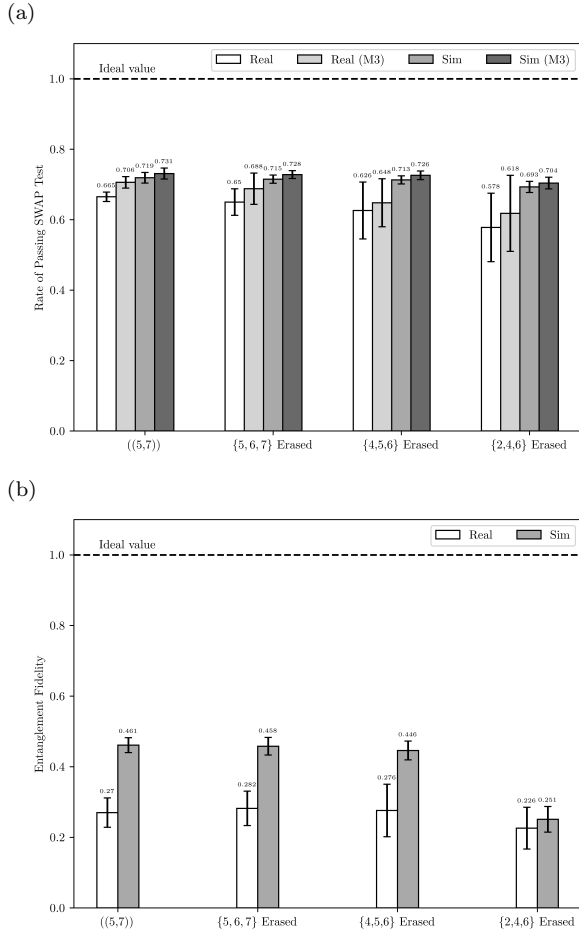


FIG. 9: (a) Sample rate of passing the SWAP test for different access structures of the Steane Code. (b) Entanglement fidelity for different access structures of the Steane Code. The numbers within the curly brackets indicate which qubits were erased. In principle, qubit sets  $\{5, 6, 7\}$  and  $\{4, 5, 6\}$  are correctable erasures while a  $\{2, 4, 6\}$  erasure is not correctable. For both figures of merit, the ideal value is the noiseless case, meaning the value measured if the schemes are run without noise present.

formed relatively close to the predictions of the noisy simulations. For the entanglement fidelity shown in Fig. 7b, we can see that noisy simulated data and real data differ significantly, at least for the  $((3,5))$  and  $((5,7))$  schemes. The low baseline fidelity we again attribute to the long idle time of qubits in our circuit, and as expected, the  $((2,3))$  scheme performs the worst due to its circuit depth. Furthermore, with respect to the baseline data, the real results have less disparity, implying that, given the IBM machine’s current ability to preserve a state at that depth without tailored error mitigation, the schemes performed well.

As shown in Fig. 8a and Fig. 8b the Steane code with two erasures, or  $((5,7))$  scheme, slightly outperformed the Steane code with three erasures in the SWAP test, however, the reverse seems to be true in regards to the

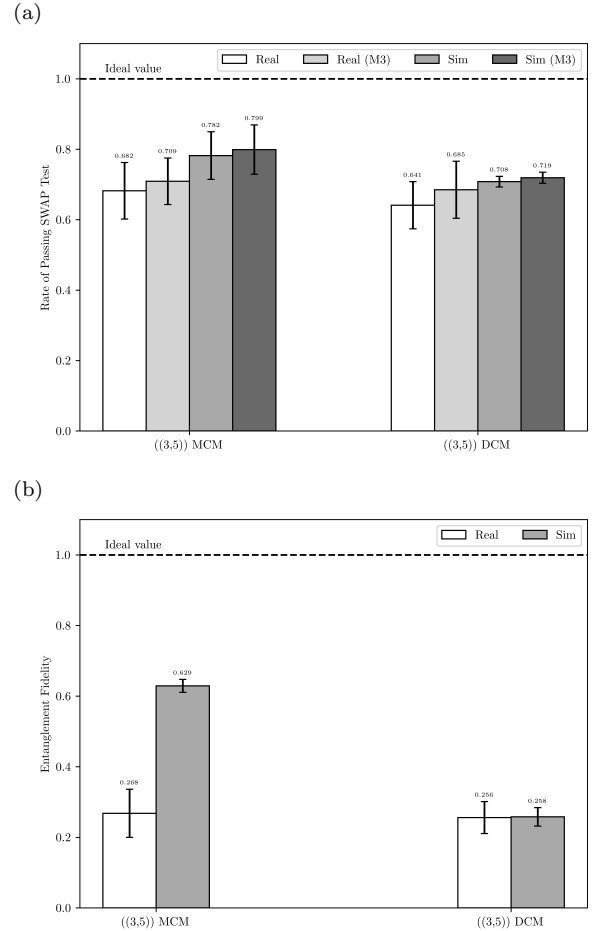


FIG. 10: (a) Sample rate of passing the SWAP test for two versions of the  $((3,5))$  threshold scheme; mid-circuit measurement versus delayed circuit measurement. (b) Entanglement fidelity for two versions of the  $((3,5))$  threshold scheme. For both figures of merit, the ideal value is the noiseless case, meaning the value measured if the schemes are run without noise present. The error bars shown correspond to a 99% confidence interval.

entanglement fidelity. This could indicate that erasing more qubits is harder to recover from but enables better preservation of entanglement. Furthermore, if we look at the comparison between different access structures of the Steane code in Fig. 9a and Fig. 9b we can see that the performance is similar across the board for the unauthorized sets. More specifically, for the  $((5,7))$  threshold scheme, all sets of two-qubit erasures can be corrected. However, in the case of three-qubit erasures, only certain subsets of parties are authorized. Specifically, qubit sets  $\{5, 6, 7\}$  and  $\{4, 5, 6\}$  are correctable erasures while  $\{2, 4, 6\}$  is not. The inability to correct from a  $\{2, 4, 6\}$  erasure is most pronounced when examining the entanglement fidelity data. Interestingly, the dip in performance in the SWAP test is less significant, which begs the question of how much noise can be tolerated before a  $\{2, 4, 6\}$  erasure becomes no more harmful than, say, a

$\{5, 6, 7\}$  erasure. Our results suggest that the IBM machines are currently performing just above this threshold.

For the  $((3,5))$  scheme, the MCM construction outperformed the DCM construction by a noticeable margin in both the SWAP test and entanglement fidelity for both real and simulated data as shown in Fig. 10a and Fig. 10b. This implies that using classical feed-forward decoding is slightly more efficient than fully coherent decoding with a delayed measurement with these schemes. This could also be another reason for the qutrit scheme’s poor performance compared to the others. Furthermore, as mentioned previously we see a large discrepancy between the real and simulated data for the entanglement fidelity of the MCM construction, however, the discrepancy is not present for the DCM construction.

## V. CONCLUSIONS AND OUTLOOK

In this paper, we provided a detailed procedure for the construction of encoding and decoding circuits for  $((3,5))$ ,  $((5,7))$ , and  $((2,3))$  threshold secret sharing schemes. We also went beyond the threshold scheme of the Steane code and investigated its more general access structure, as well as comparing different measurement implementations (MCM vs DCM). The ultimate goal of this work was twofold. First, we wanted to provide a quantum circuit description of quantum secret sharing in an introductory manner that might be useful to newcomers to the field. Second, we wanted to see how well certain QSS schemes perform on a commercial quantum computing platform such as IBM’s 127-qubit Brisbane system. While we used M3 error mitigation to improve some of our data, the scope of this work was just to obtain a benchmarking performance of the IBM machine for the task of secret sharing, as it is currently available to the user.

There are multiple reasons for the discrepancies between the ideal, simulated, and real data. As noted above, we believe the primary source for non-ideal performance in the SWAP test and entanglement fidelity estimation is the depth of our circuits and consequently the decoherence of idle qubits. A natural next step would be to employ more tailored error mitigation techniques such as dynamical decoupling, as pursued in Refs. [39], especially to help with the additional wait time required to perform mid-circuit measurements. Another direction would be to look at machines with different basis (native) gates. Different basis gate sets could improve the performance of the schemes by decreasing the transpilation requirements. For IBM machines specifically, this would require running the schemes on machines with processors other than ones with “Eagle” processors, e.g., “Heron.”

Regarding the differences between the simulated and real data, we suspect that this is partially due to the limitations of the fake backend in the simulation. The error rates and noise programmed into a fake backend only represent a snapshot of what one would see on real

hardware. On a real quantum device, the error rates and noise can change dynamically, and the qubits can experience more cross-talk. This will have more deleterious effects as the number of qubits increases, which is the case when estimating the entanglement fidelity since an extra reference system is introduced to hold part of the entanglement.

## ACKNOWLEDGMENTS

We wish to acknowledge the support of the National Science Foundation Research Experience for Undergraduates (REU) program (Grant PHY-2112890) for funding this research, as well as the IBM-Illinois Discovery Accelerator Institute. E.C. is also very grateful to Alireza Seif for discussing different error mitigation techniques on IBM machines. We would also like to thank Sarah Hagen for useful discussions.

### Appendix A: $[[7,1,3]]$ Steane code and three-qubit erasures

When doing our analysis of the  $[[7,1,3]]$  Steane code and the expected admission of a  $((5,7))$  threshold scheme we came across the fact that the Steane code could recover from  $d = 3$  erasures of certain qubits. We show that a subset of three qubits exists in a maximally mixed state, which implies that these qubits are independent of the logical state. Consequently, the remaining four qubits must contain all the information about the original encoded quantum state.

The encoded state is:

$$|\psi\rangle_L = \frac{\alpha}{\sqrt{8}} \sum_{i=1}^8 |u_i\rangle + \frac{\beta}{\sqrt{8}} \sum_{j=1}^8 |v_j\rangle. \quad (\text{A0})$$

Where:

$$|u_i\rangle : |0000000\rangle, |1010101\rangle, |0110011\rangle, |1100110\rangle, \\ |0001111\rangle, |1011010\rangle, |0111100\rangle, |1101001\rangle$$

$$|v_j\rangle : |1111111\rangle, |0101010\rangle, |1001100\rangle, |0011001\rangle, \\ |1110000\rangle, |0100101\rangle, |1000011\rangle, |0010110\rangle.$$

Furthermore, the full density matrix  $\rho$  is:

$$\rho = |\psi\rangle\langle\psi|_L \quad (\text{A1})$$

To find the reduced density matrix for the set of qubits,  $S = \{q_5, q_6, q_7\}$ , we must first trace out  $\bar{S} = \{q_1, q_2, q_3, q_4\}$  from the encoded state  $|\psi\rangle_L$ :

$$\rho^S = \text{tr}_{\bar{S}}(|\psi\rangle\langle\psi|_L) = \sum_{i,j,k,l=0}^1 \langle ijkl|\rho|ijkl\rangle \quad (\text{A2})$$



TABLE V: For arbitrary Pauli errors on qubits five, six, and seven in the Steane QSS scheme, this table provides the unitary correction  $R_k$  on qubit one for each syndrome measurement  $\mathbf{b}_k$ .

Error	Syndrome	Correction	Error	Syndrome	Correction
$\mathbb{I}_5\mathbb{I}_6\mathbb{I}_7$	(0, 0, 0, 0, 0, 0)	$\mathbb{I}_1$	$Y_5\mathbb{I}_6\mathbb{I}_7$	(1, 1, 1, 1, 0, 0)	$\mathbb{I}_1$
$\mathbb{I}_5\mathbb{I}_6X_7$	(0, 1, 1, 0, 0, 0)	$X_1$	$Y_5\mathbb{I}_6X_7$	(1, 0, 0, 1, 0, 0)	$X_1$
$\mathbb{I}_5\mathbb{I}_6Y_7$	(0, 1, 1, 0, 0, 1)	$X_1$	$Y_5\mathbb{I}_6Y_7$	(1, 0, 0, 1, 0, 1)	$X_1$
$\mathbb{I}_5\mathbb{I}_6Z_7$	(0, 0, 0, 0, 0, 1)	$\mathbb{I}_1$	$Y_5\mathbb{I}_6Z_7$	(1, 1, 1, 1, 0, 1)	$\mathbb{I}_1$
$\mathbb{I}_5X_6\mathbb{I}_7$	(1, 0, 1, 0, 0, 0)	$X_1$	$Y_5X_6\mathbb{I}_7$	(0, 1, 0, 1, 0, 0)	$X_1$
$\mathbb{I}_5X_6X_7$	(1, 1, 0, 0, 0, 0)	$\mathbb{I}_1$	$Y_5X_6X_7$	(0, 0, 1, 1, 0, 0)	$\mathbb{I}_1$
$\mathbb{I}_5X_6Y_7$	(1, 1, 0, 0, 0, 1)	$\mathbb{I}_1$	$Y_5X_6Y_7$	(0, 0, 1, 1, 0, 1)	$\mathbb{I}_1$
$\mathbb{I}_5X_6Z_7$	(1, 0, 1, 0, 0, 1)	$X_1$	$Y_5X_6Z_7$	(0, 1, 0, 1, 0, 1)	$X_1$
$\mathbb{I}_5Y_6\mathbb{I}_7$	(1, 0, 1, 0, 1, 0)	$X_1$	$Y_5Y_6\mathbb{I}_7$	(0, 1, 0, 1, 1, 0)	$X_1$
$\mathbb{I}_5Y_6X_7$	(1, 1, 0, 0, 1, 0)	$\mathbb{I}_1$	$Y_5Y_6X_7$	(0, 0, 1, 1, 1, 0)	$\mathbb{I}_1$
$\mathbb{I}_5Y_6Y_7$	(1, 1, 0, 0, 1, 1)	$\mathbb{I}_1$	$Y_5Y_6Y_7$	(0, 0, 1, 1, 1, 1)	$\mathbb{I}_1$
$\mathbb{I}_5Y_6Z_7$	(1, 0, 1, 0, 1, 1)	$X_1$	$Y_5Y_6Z_7$	(0, 1, 0, 1, 1, 1)	$X_1$
$\mathbb{I}_5Z_6\mathbb{I}_7$	(0, 0, 0, 0, 1, 0)	$\mathbb{I}_1$	$Y_5Z_6\mathbb{I}_7$	(1, 1, 1, 1, 1, 0)	$\mathbb{I}_1$
$\mathbb{I}_5Z_6X_7$	(0, 1, 1, 0, 1, 0)	$X_1$	$Y_5Z_6X_7$	(1, 0, 0, 1, 1, 0)	$X_1$
$\mathbb{I}_5Z_6Y_7$	(0, 1, 1, 0, 1, 1)	$X_1$	$Y_5Z_6Y_7$	(1, 0, 0, 1, 1, 1)	$X_1$
$\mathbb{I}_5Z_6Z_7$	(0, 0, 0, 0, 1, 1)	$\mathbb{I}_1$	$Y_5Z_6Z_7$	(1, 1, 1, 1, 1, 1)	$\mathbb{I}_1$
$X_5\mathbb{I}_6\mathbb{I}_7$	(1, 1, 1, 0, 0, 0)	$\mathbb{I}_1$	$Z_5\mathbb{I}_6\mathbb{I}_7$	(0, 0, 0, 1, 0, 0)	$\mathbb{I}_1$
$X_5\mathbb{I}_6X_7$	(1, 0, 0, 0, 0, 0)	$X_1$	$Z_5\mathbb{I}_6X_7$	(0, 1, 1, 1, 0, 0)	$X_1$
$X_5\mathbb{I}_6Y_7$	(1, 0, 0, 0, 0, 1)	$X_1$	$Z_5\mathbb{I}_6Y_7$	(0, 1, 1, 1, 0, 1)	$X_1$
$X_5\mathbb{I}_6Z_7$	(1, 1, 1, 0, 0, 1)	$\mathbb{I}_1$	$Z_5\mathbb{I}_6Z_7$	(0, 0, 0, 1, 0, 1)	$\mathbb{I}_1$
$X_5X_6\mathbb{I}_7$	(0, 1, 0, 0, 0, 0)	$X_1$	$Z_5X_6\mathbb{I}_7$	(1, 0, 1, 1, 0, 0)	$X_1$
$X_5X_6X_7$	(0, 0, 1, 0, 0, 0)	$\mathbb{I}_1$	$Z_5X_6X_7$	(1, 1, 0, 1, 0, 0)	$\mathbb{I}_1$
$X_5X_6Y_7$	(0, 0, 1, 0, 0, 1)	$\mathbb{I}_1$	$Z_5X_6Y_7$	(1, 1, 0, 1, 0, 1)	$\mathbb{I}_1$
$X_5X_6Z_7$	(0, 1, 0, 0, 0, 1)	$X_1$	$Z_5X_6Z_7$	(1, 0, 1, 1, 0, 1)	$X_1$
$X_5Y_6\mathbb{I}_7$	(0, 1, 0, 0, 1, 0)	$X_1$	$Z_5Y_6\mathbb{I}_7$	(1, 0, 1, 1, 1, 0)	$X_1$
$X_5Y_6X_7$	(0, 0, 1, 0, 1, 0)	$\mathbb{I}_1$	$Z_5Y_6X_7$	(1, 1, 0, 1, 1, 0)	$\mathbb{I}_1$
$X_5Y_6Y_7$	(0, 0, 1, 0, 1, 1)	$\mathbb{I}_1$	$Z_5Y_6Y_7$	(1, 1, 0, 1, 1, 1)	$\mathbb{I}_1$
$X_5Y_6Z_7$	(0, 1, 0, 0, 1, 1)	$X_1$	$Z_5Y_6Z_7$	(1, 0, 1, 1, 1, 1)	$X_1$
$X_5Z_6\mathbb{I}_7$	(1, 1, 1, 0, 1, 0)	$\mathbb{I}_1$	$Z_5Z_6\mathbb{I}_7$	(0, 0, 0, 1, 1, 0)	$\mathbb{I}_1$
$X_5Z_6X_7$	(1, 0, 0, 0, 1, 0)	$X_1$	$Z_5Z_6X_7$	(0, 1, 1, 1, 1, 0)	$X_1$
$X_5Z_6Y_7$	(1, 0, 0, 0, 1, 1)	$X_1$	$Z_5Z_6Y_7$	(0, 1, 1, 1, 1, 1)	$X_1$
$X_5Z_6Z_7$	(1, 1, 1, 0, 1, 1)	$\mathbb{I}_1$	$Z_5Z_6Z_7$	(0, 0, 0, 1, 1, 1)	$\mathbb{I}_1$

- 
- [1] R. Cleve, D. Gottesman, and H.-K. Lo, How to share a quantum secret, *Phys. Rev. Lett.* **83**, 648 (1999).
- [2] G. R. Blakley, Safeguarding cryptographic keys, in *1979 International Workshop on Managing Requirements Knowledge (MARK)* (1979) pp. 313–318.
- [3] A. Shamir, How to share a secret, *Commun. ACM* **22**, 612–613 (1979).
- [4] M. Hillery, V. Bužek, and A. Berthiaume, Quantum secret sharing, *Physical Review A* **59**, 1829–1834 (1999).
- [5] D. Gottesman, Theory of quantum secret sharing, *Phys. Rev. A* **61**, 042311 (2000).
- [6] A. D. Smith, Quantum secret sharing for general access structures (2000), arXiv:quant-ph/0001087 [quant-ph].
- [7] A. C. A. Nascimento, J. Mueller-Quade, and H. Imai, Improving quantum secret-sharing schemes, *Phys. Rev. A* **64**, 042311 (2001).
- [8] H. Imai, J. Mueller-Quade, A. Nascimento, P. Tuyls, and A. Winter, A quantum information theoretical model for quantum secret sharing schemes, *Quantum Information & Computation* **5**, 10.26421/QIC5.1-7 (2003).
- [9] D. Markham and B. C. Sanders, Graph states for quantum secret sharing, *Phys. Rev. A* **78**, 042309 (2008).
- [10] P. Sarvepalli, Bounds on the information rate of quantum-secret-sharing schemes, *Phys. Rev. A* **83**, 042324 (2011).
- [11] V. Gheorghiu, Generalized semiquantum secret-sharing schemes, *Phys. Rev. A* **85**, 052309 (2012).
- [12] B. Fortescue and G. Gour, Reducing the quantum communication cost of quantum secret sharing, *IEEE Transactions on Information Theory* **58**, 6659 (2012).
- [13] W. Yang, L. Huang, R. Shi, and L. He, Secret sharing based on quantum fourier transform, *Quantum Information Processing* **12**, 2465 (2013).
- [14] V. Gheorghiu and B. C. Sanders, Accessing quantum secrets via local operations and classical communication, *Phys. Rev. A* **88**, 022340 (2013).
- [15] A. Marin and D. Markham, Equivalence between sharing quantum and classical secrets and error correction, *Phys. Rev. A* **88**, 042332 (2013).
- [16] L. Li, D. Qiu, and P. Mateus, Quantum secret sharing with classical bobs, *Journal of Physics A: Mathematical and Theoretical* **46**, 045304 (2013).
- [17] Y. Ouyang, S.-H. Tan, L. Zhao, and J. F. Fitzsimons, Computing on quantum shared secrets, *Phys. Rev. A* **96**, 052333 (2017).
- [18] V. Lipinska, G. Murta, J. Ribeiro, and S. Wehner, Verifiable hybrid secret sharing with few qubits, *Phys. Rev. A* **101**, 032332 (2020).
- [19] K. Senthoo and P. K. Sarvepalli, Theory of communication efficient quantum secret sharing, *IEEE Transactions on Information Theory* **68**, 3164 (2022).
- [20] Y. Ouyang, K. Goswami, J. Romero, B. C. Sanders, M.-H. Hsieh, and M. Tomamichel, Approximate reconstructability of quantum states and noisy quantum secret sharing schemes, *Phys. Rev. A* **108**, 012425 (2023).
- [21] W. Tittel, H. Zbinden, and N. Gisin, Experimental demonstration of quantum secret sharing, *Phys. Rev. A* **63**, 042301 (2001).
- [22] S. Gaertner, C. Kurtsiefer, M. Bourennane, and H. Weinfurter, Experimental demonstration of four-party quantum secret sharing, *Phys. Rev. Lett.* **98**, 020503 (2007).
- [23] L. Hao, C. Wang, and G. L. Long, Quantum secret sharing protocol with four state grover algorithm and its proof-of-principle experimental demonstration, *Optics Communications* **284**, 3639 (2011).
- [24] K.-J. Wei, H.-Q. Ma, and J.-H. Yang, Experimental circular quantum secret sharing over telecom fiber network, *Optics Express* **21**, 16663 (2013).
- [25] B. A. Bell, D. Markham, D. A. Herrera-Martí, A. Marin, W. J. Wadsworth, J. G. Rarity, and M. S. Tame, Experimental demonstration of graph-state quantum secret sharing, *Nature Communications* **5**, doi:10.1038/ncomms6480 (2014).
- [26] H. Lu, Z. Zhang, L.-K. Chen, Z.-D. Li, C. Liu, L. Li, N.-L. Liu, X. Ma, Y.-A. Chen, and J.-W. Pan, Secret sharing of a quantum state, *Phys. Rev. Lett.* **117**, 030501 (2016).
- [27] B. P. Williams, J. M. Lukens, N. A. Peters, B. Qi, and W. P. Grice, Quantum secret sharing with polarization-entangled photon pairs, *Phys. Rev. A* **99**, 062311 (2019).
- [28] S. M. Lee, S.-W. Lee, H. Jeong, and H. S. Park, Quantum teleportation of shared quantum secret, *Phys. Rev. Lett.* **124**, 060501 (2020).
- [29] M. de Oliveira, I. Nape, J. Pinnell, N. TabeBordbar, and A. Forbes, Experimental high-dimensional quantum secret sharing with spin-orbit-structured photons, *Phys. Rev. A* **101**, 042303 (2020).
- [30] D. Suter and G. A. Álvarez, Colloquium: Protecting quantum information against environmental noise, *Rev. Mod. Phys.* **88**, 041001 (2016).

- [31] M. A. Nielsen and I. L. Chuang, *Quantum Computation and Quantum Information: 10th Anniversary Edition* (Cambridge University Press, 2011).
- [32] R. Laflamme, C. Miquel, J. P. Paz, and W. H. Zurek, Perfect quantum error correcting code, *Phys. Rev. Lett.* **77**, 198 (1996).
- [33] A. R. Calderbank and P. W. Shor, Good quantum error-correcting codes exist, *Phys. Rev. A* **54**, 1098 (1996).
- [34] A. Steane, Multiple-particle interference and quantum error correction, *Proceedings of the Royal Society of London. Series A: Mathematical, Physical and Engineering Sciences* **452**, 2551 (1996).
- [35] R. Majumdar and S. Sur-Kolay, Optimal error correcting code for ternary quantum systems (2020), arXiv:1906.11137 [quant-ph].
- [36] M. Grassl, T. Beth, and T. Pellizzari, Codes for the quantum erasure channel, *Phys. Rev. A* **56**, 33 (1997).
- [37] P. D. Nation, H. Kang, N. Sundaresan, and J. M. Gambetta, Scalable mitigation of measurement errors on quantum computers, *PRX Quantum* **2**, 040326 (2021).
- [38] P. Sarvepalli, Nonthreshold quantum secret-sharing schemes in the graph-state formalism, *Phys. Rev. A* **86**, 042303 (2012).
- [39] E. Bäumer, V. Tripathi, A. Seif, D. Lidar, and D. S. Wang, Quantum fourier transform using dynamic circuits (2024), arXiv:2403.09514 [quant-ph].